IJAME

Int. J. of Applied Mechanics and Engineering, 2026, vol.31, No.1, pp.XXX-XXX
DOI: 10.59441/ijame/223944

CHAOTIC THERMOSOLUTAL CONVECTION IN A ROTATING POROUS CAVITY SATURATED WITH NEWTONIAN FLUID

V.M. Kpeho[1*] and A.L. Hinvi[2]
[1]Ecole Doctorale des Sciences Technologies Ingénierie et Mathématiques, Laboratoire des Procédés et de l'Innovation Technologique, Institut National Supérieur de Technologie Industrielle, Université Nationale des Sciences, Technologies, Ingénierie et Mathématiques d'Abomey, Bénin, BENIN
[2]Département de Génie Mécanique et Productique, Laboratoire des Procédés et de l'Innovation Technologique, Institut National Supérieur de Technologie Industrielle, Université Nationale des Sciences, Technologies, Ingénierie et Mathématiques d'Abomey, Bénin, BENIN
E-mail: hinvi.laurent@unstim.bj

The various transitions that can occur during thermosolutal convection in a saturated porous cavity filled with a Newtonian fluid are examined in this work in order to evaluate the effects of pores, solute concentration, and rotational force on this flow. To convert the linked equations into a six-dimensional system of nonlinear equations, we used a minimum-order double Fourier series method in line with Galerkin's truncated approximation. This resulting dynamical system is numerically solved using the fourth-order Runge-Kutta method. The analytical computations are consolidated using phase spaces, time histories, bifurcation diagrams, and Lyapunov diagrams. The findings demonstrate the linear, chaotic, and period-doubling tendencies of fluid flow. In contrast to the situation of a Newtonian fluid, numerical computations have demonstrated that the existence of a solute concentration in a Newtonian fluid subjected to a rotational force postpones the onset of chaos and periodic convection. Numerical calculations demonstrate that various parameters such as porosity, solute concentration, and rotation significantly influence thermosolutal flow. These results have practical implications in several technical and geophysical applications, such as enhanced oil recovery, geothermal energy extraction, chemical reactors, and heat and mass transfer processes in porous media.

Keywords: chaos, bifurcation, dynamic system, double-diffuse convection.

1. Introduction

Thermal convection in porous media is a fundamental phenomenon with substantial applications in geosciences, process engineering, and heat transfer technologies [1]. When a porous medium is saturated with a fluid and exposed to a temperature differential, convection cells can form, influencing crucial processes such as geothermal energy extraction, nuclear waste storage, and others [2, 3]. Nield [4] was the first to investigate the regular stability theory of this type of fluid flow, using examples such as thermosolutal convection in porous media used during binary mixture solidification, solute migration in water-saturated soils, geophysical systems, electrochemistry, and moisture migration through the air contained in fibrous insulators [5]. He demonstrated that oscillatory instability can occur when a strongly stabilizing solute gradient opposes a destabilizing thermal gradient, and that the stability limit differs significantly from a straight line when the critical thermal wave number differs considerably from the critical wave number of the solute. This analysis was further investigated by Taunton *et al.* [6]. They studied the case of saline finger thermoconvection while characterizing the main differences in the dependence of the solute Rayleigh number on the wave number at the regular state and in the dependence of the horizontal wave number in the saline fingers region of regular stability of convective heat transfer on the thermal and solute Rayleigh numbers. Several other detailed studies have also been conducted on thermosolutal convective heat transfer in porous media, such as the work of Mojtabi and Charrier-Mojtabi [7] and Mamou [8]. A fluid containing suspended particles offers numerous engineering applications, particularly in the context of double-diffuse convective heat transfer. A notable example is the solar pond, where the presence of suspended particles significantly enhances energy storage efficiency. In a solar pond with a clear fluid, heat energy cannot be retained for extended periods. To address this limitation, suspended particles are introduced, enabling more effective energy storage. Furthermore, research on transitions to chaos in two-dimensional convection with double diffusion began after the work of Huppert [9, 10]. The latter misinterpreted the bifurcation towards asymmetry as a period-doubling bifurcation of transitions between periodic and chaotic oscillations in thermosolutal convection. Knobloch [11] then conducted a more systematic study of these transitions and demonstrated that they occur through a cascade of period-doubling bifurcations. They found that the onset of chaotic convection is associated with homoclinic and heteroclinic bifurcations where the oscillatory branch meets the unstable part of the stable branch with increasing Rayleigh number. Some properties of two-dimensional stochastic regimes of thermosolutal convection are investigated by Sibgatullin et *al.* [12]. They demonstrated that the structure of the attraction collector varies as a function of the thermal and solutal Rayleigh numbers. Recently, Idris *et al.* [13] studied a chaotic system resulting from double-diffusive convection in a fluid layer based on a five-dimensional dynamical system. By varying system parameters such as Rayleigh number and Lewis number, they noticed that the trajectory of the data points indicated a sequence of period changes, and that the behavior remained the same when the Rayleigh number was higher. Sharma et *al.* [14] added that energy and solute profiles are improved by thermal radiation in conjunction with reactive species. The increase in Reynolds number and temperature ratio leads to an increase in the entropy of the fluid flow, but this is controlled by the radiation parameters [15].

Thermosolutal convection in Newtonian fluids plays an important role in natural and technical processes such as groundwater flow, oil recovery, and chemical reactors, where porous media and rotational effects play a key role. Studying chaos in this context provides insight into the dynamics of nonlinear and unpredictable behaviors that can occur and affect the efficiency of heat and mass transport, which is essential for system optimization. Porous cavities and rotation add complexity that is relevant to many industrial and environmental applications where fluids saturate porous structures and are subject to Coriolis forces.

The objective of this paper is to extend this work by taking into account the effect of pores and rotational force on thermosolute fluid flow. In this study, the novelty lies in the fact that, considering the porosity of the cavity and the rotational force, the truncated Galerkin approximation allows us to obtain a robust system with six ordinary differential equations, as opposed to the three, four, and five equations commonly found in the literature. We wish to study the effects of medium porosity, mass diffusion, and rotational force on the flow of thermosoluble fluid. To this end in section two, we model the flow of a thermosolutal fluid by partial differential equations of mass conservation, Navier Stockes, heat-flux and concentration, which are transformed into ordinary differential equations using truncated Galerkin transformations. In section three, resulting system of nonlinear equations is analyzed according to dynamical systems theory. The section four is devoted to the results and discussions and we finish with the conclusion in the fifth section.

2. Basic equations governing thermosolute convection

Let's consider a saturated porous horizontal layer of thermosolutal fluid, incompressible and rotating at constant speed Ω around a vertical axis. The two infinitely extended horizontal plates are subjected to a vertical gradient of temperatures and concentrations across the fluid, so that the upper plate at temperature $T_h = T_0$ and concentration $S_h = S_0$, and the lower plate at temperature $T_l = T_0 + \Delta T$ and concentration $S_h = S_0 + \Delta S$. An orthonormal Cartesian coordinate system is adopted so that its origin coincides with the lower boundary of the domain and its *z* axis is vertical. Thermal, mechanical and solubility properties in the x and y directions are assumed to be identical. Flow obeys the law of Darcy and taking into account Boussinesq's approximations, density can be described as:

$$\rho = \rho_0 \left[1 - \alpha_T \left(T - T_C \right) + \alpha_S \left(S - S_C \right) \right], \tag{2.1}$$

where α_T and α_S are volume dilatation coefficients due to variations in temperature and solute concentration. The geometry of this considered problem is presented in Fig.1.

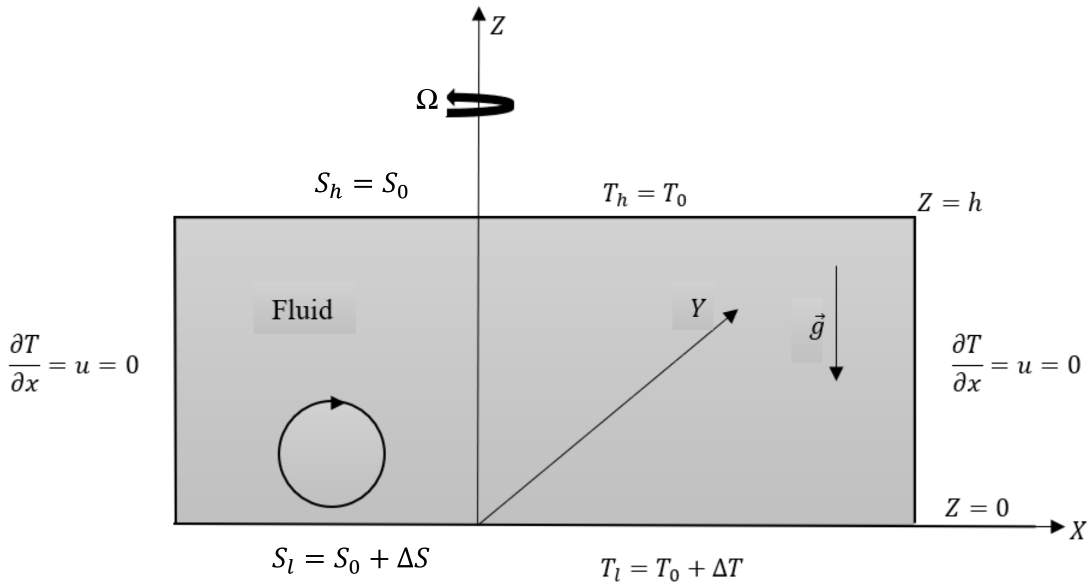

Fig.1. Schematic diagram of the problem.

Therefore, thermosolutal fluid flow in the horizontal, infinite porous cavity are modeling by the set of moving equations of the conservation of mass, conservation of momentum, energy and solute concentration, given by:

$$\nabla . q = 0, \tag{2.2}$$

$$\frac{\rho_0}{\Phi}\frac{\partial q}{\partial t} + 2\frac{\rho_0}{\Phi}\Omega \times q = -\nabla p - \frac{\mu_0}{k}q + \rho g, \tag{2.3}$$

$$\frac{\partial T}{\partial t} + (q.\nabla)T = k_T \nabla^2 T, \tag{2.4}$$

$$\frac{\partial S}{\partial t} + (q.\nabla)S = k_S \nabla^2 S, \tag{2.5}$$

where, k and Φ are the permeability and the porosity of the cavity and μ_0 the fluid dynamic viscosity. When the fluid is at rest or the flow is uniform, the time-independent solution of the flow equations with temperature and heat flux varying only in the z-direction is given by:

$$T_b = T_0 + \Delta T\left(1 - \frac{z}{h}\right) \quad \text{and} \quad S_b = S_0 + \Delta S\left(1 - \frac{z}{h}\right). \tag{2.6}$$

The basic solutions are disturbed by taking the quantities in the following forms:

$$q = q_b + q', \quad p = p_b(z) + p', \quad T = T_b(z) + T', \quad \rho = \rho_0(z) + \rho', \quad S = S_b(z) + S'. \tag{2.7}$$

Substituting these perturbation equations into Eqs (2.2)-(2.5) and applying the perturbation conditions, we obtain the following equations after ignoring the primes:

$$\nabla . q = 0 , \tag{2.8}$$

$$\frac{\rho_0}{\Phi}\frac{\partial q}{\partial t} = -\nabla p - \frac{\mu_0}{k} q + \rho g + 2\frac{\rho_0}{\Phi}\Omega \times q , \tag{2.9}$$

$$\frac{\partial T}{\partial t} + (q.\nabla) T_b = k_T \nabla^2 T , \tag{2.10}$$

$$\frac{\partial S}{\partial t} + (q.\nabla) S_b = k_S \nabla^2 S . \tag{2.11}$$

For the parametric representation of fluid, which allows us to determine the characteristic properties of the system, we reformulate the flow equations taking into account the following normalized quantities:

$$(x, y, z) = h\left(x^*, y^*, z^*\right), \quad q = \frac{k_T}{h} q^*, \quad t = \frac{h^2}{k_T} t^*,$$
$$p = \frac{\mu_0 k_T}{h^2} p^*, \quad T^* = \frac{T - T_c}{\Delta T} , \quad S^* = \frac{S - S_C}{\Delta S} . \tag{2.12}$$

In this case, we obtain:

$$\nabla^* q^* = 0 , \tag{2.13}$$

$$\frac{1}{\Phi}\frac{k_T}{\nu_0}\frac{\partial q^*}{\partial t^*} = -\nabla^* p^* - \frac{h^2}{k_T} q^* - 2\frac{\Omega h^2}{\Phi \nu_0} q^* e_z + \frac{g h^3 \alpha_T \Delta T}{\nu_0 k_T} T^* e_z - \frac{g h^3 \alpha_S \Delta S}{\nu_0 k_T} S^* e_z , \tag{2.14}$$

$$\frac{\partial T}{\partial t} + (q.\nabla) T_b + (q\nabla) T = k_T \nabla^2 T , \tag{2.15}$$

$$\frac{\partial S}{\partial t} + (q.\nabla) S_b + (q\nabla) S = k_S \nabla^2 S . \tag{2.16}$$

In Eqs (2.12)-(2.16), we have dimensionless whose expressions are as follows:

$$Da = \frac{k}{h^2}, \quad Pr = \frac{\nu_0}{k_T}, \quad Le = \frac{k_T}{k_S} , \quad Va = \frac{\Phi Pr}{Da} , \tag{2.17}$$

$$Ta = \frac{4\Omega^2 h^4}{\nu_0{}^2}, \quad Ra = \frac{g h \alpha_T \Delta T}{\nu_0}, \quad Rs = \frac{g h^3 \alpha_S \Delta S}{\nu_0} . \qquad \text{(2.17 cont.)}$$

Which are, respectively, the Darcy number, the Prandtl number, the Lewis number, the Vadasz number, the Taylor number, the Rayleigh number and the solutal Rayleigh number. This allows us rewrite the momentum, heat-flux and concentration equations in a dimensionless from:

$$\left(\frac{1}{Va}\frac{\partial}{\partial t}+1\right)q=-Da\nabla p-\frac{Da\sqrt{Ta}}{\Phi}qe_z+RaDaTe_z-RsDaSe_z, \tag{2.18}$$

$$\frac{\partial T}{\partial t}+\left(q\nabla\right)T_b+\left(q\nabla\right)T=\nabla^2 T, \tag{2.19}$$

$$\frac{\partial S}{\partial t}+\left(q.\nabla\right)S_b+\left(q\nabla\right)S=\frac{1}{Le}\nabla^2 S. \tag{2.20}$$

We now eliminate the pressure from the dimensionless equations by applying the curl-curl, the vorticity equations allows us to write:

$$\begin{aligned}-\left(\frac{1}{Va}\frac{\partial}{\partial t}+1\right)^2\nabla^2\omega=\left(\frac{Da\sqrt{Ta}}{\Phi}\right)^2\frac{\partial^2\omega}{\partial z^2}-RaDa\left(\frac{1}{Va}\frac{\partial}{\partial t}+1\right)\left(\frac{\partial^2 T}{\partial x^2}+\frac{\partial^2 T}{\partial y^2}\right)+\\+RsDa\left(\frac{1}{Va}\frac{\partial}{\partial t}+1\right)\left(\frac{\partial^2 S}{\partial x^2}+\frac{\partial^2 S}{\partial y^2}\right).\end{aligned} \tag{2.21}$$

Given that there is no movement on the y-axis, we have:

$$\left[\left(\frac{1}{Va}\frac{\partial}{\partial t}+1\right)^2\nabla^2+\frac{Da^2Ta}{\Phi^2}\frac{\partial^2}{\partial z^2}\right]\omega=RaDa\left(\frac{1}{Va}\frac{\partial}{\partial t}+1\right)\frac{\partial^2 T}{\partial x^2}-RsDa\left(\frac{1}{Va}\frac{\partial}{\partial t}+1\right)\frac{\partial^2 S}{\partial x^2}. \tag{2.22}$$

Expressing the vertical component of velocity as a current function, $\omega=\frac{\partial\Psi}{\partial t}$, the previous equation gives:

$$\left[\left(\frac{1}{Va}\frac{\partial}{\partial t}+1\right)^2\nabla^2+\frac{Da^2Ta}{\Phi^2}\frac{\partial^2}{\partial z^2}\right]\frac{\partial\Psi}{\partial t}=RaDa\left(\frac{1}{Va}\frac{\partial}{\partial t}+1\right)\frac{\partial^2 T}{\partial x^2}-RsDa\left(\frac{1}{Va}\frac{\partial}{\partial t}+1\right)\frac{\partial^2 S}{\partial x^2}. \tag{2.23}$$

The temperature and concentration equations become:

$$\left(\frac{\partial}{\partial t}-\nabla^2\right)T=\frac{\partial\Psi}{\partial x}+\frac{\partial\Psi}{\partial z}\frac{\partial T}{\partial x}-\frac{\partial\Psi}{\partial x}\frac{\partial T}{\partial z}, \tag{2.24}$$

$$\left(\frac{\partial}{\partial t}-\nabla^2\right)S=\frac{\partial\Psi}{\partial x}+\frac{\partial\Psi}{\partial z}\frac{\partial S}{\partial x}-\frac{\partial\Psi}{\partial x}\frac{\partial S}{\partial z}. \tag{2.25}$$

3. Analysis of the dynamic behavior of the flow

To perform a linear stability analysis of the thermosolutal convection, let us consider that the velocity components, temperature and solute can be represented as a sum of double-Fourier series according to the work of Saltzman *et al.* [16]:

$$\Psi(\tau,x,z)=\sum_{n=1}^{\infty}\sum_{m=1}^{\infty}A_{m,n}(\tau)\sin(\max)\sin(n\pi z), \tag{3.1}$$

$$T(\tau,x,z)=\sum_{n=1}^{\infty}\sum_{m=1}^{\infty}B_{m,n}(\tau)\cos(\max)\sin(n\pi z), \tag{3.2}$$

$$S(\tau,x,z)=\sum_{n=1}^{\infty}\sum_{m=1}^{\infty}C_{m,n}(\tau)\cos(\max)\sin(n\pi z). \tag{3.3}$$

Further, we consider the modes $m=1$ and $n=1$ for stream function, and the modes $(0,2)$ and $(1,1)$ for temperature, and solute concentration which represent the minimal Galerkin expansion:

$$\Psi = A_1 sin(ax)sin(\pi z), \tag{3.4}$$

$$T = B_1 cos(ax)sin(\pi z)+B_2 sin(2\pi z), \tag{3.5}$$

$$S = C_1 cos(ax)sin(\pi z)+C_2 sin(2\pi z). \tag{3.6}$$

An additional mode introduced for temperature and solute concentration is called the convective mode. The modes represent slight deviations in the average profile (i.e., the horizontal average) caused by convective flow. The amplitudes A_1, B_1, B_2, C_1, and C_2 are aligned with the nonlinear interactions. Equations (3.4)-(3.6) are substituted into Eqs (2.23)-(2.25) to obtain the following nonlinear equations:

$$\begin{cases} \dfrac{\partial^2 A_1}{\partial t^2}=-2V_a\dfrac{\partial A_1}{\partial t}-V_a^2\left(1+\dfrac{Da^2Ta}{\phi^2}\dfrac{\pi^2}{a^2+\pi^2}\right)A_1+ \\ +\dfrac{aR_aV_aD_a}{a^2+\pi^2}\left(\dfrac{\partial B_1}{\partial t}+V_aB_1\right)-\dfrac{aR_SV_aD_a}{a^2+\pi^2}\left(\dfrac{\partial C_1}{\partial t}+V_aC_1\right), \\ \dfrac{\partial B_1}{\partial t}=-\left(a^2+\pi^2\right)B_1+aA_1+a\pi A_1B_2, \\ \dfrac{\partial B_2}{\partial t}-4\pi^2B_2-\dfrac{1}{2}a\pi A_1B_1, \\ \dfrac{\partial C_1}{\partial t}=-\dfrac{1}{L_e}\left(a^2+\pi^2\right)C_1+aA_1+a\pi A_1C_2, \end{cases} \tag{3.7}$$

$$\left\{\frac{\partial B_2}{\partial t} = -4\pi^2 C_2 - \frac{1}{2} a\pi A_1 C_1 .\right. \tag{3.7 cont.}$$

To simplify the system (3.7), the time, some non-dimensional parameters of the equations in the system in Eq.(3.7) should be rescaled, and the following notations are introduced as follows:

$$k^2 = \left(a^2 + \pi^2\right), \quad t' = k^2 t, \quad Ra_c = Rs_c = \frac{k^6}{a^2} \quad R = \frac{a^2 R_a}{k^6} = \frac{Ra}{Ra_c},$$
$$R_S^* = \frac{a^2 R_s}{k^6} = \frac{R_S}{R_{Sc}}, \quad T = \frac{\pi^2 T_a}{k^6}, \quad Pr = \frac{DaVa}{\Phi}, \quad a_{cr} = \frac{\pi}{\sqrt{2}}, \quad b = \frac{8}{\left(\frac{a}{a_{cr}}\right)^2 + 2}, \tag{3.8}$$

and the rescaled amplitudes:

$$A_1 = \frac{k^2\sqrt{2}}{a\pi} A_1, \quad B_1 = \frac{\sqrt{2}}{\pi R} B_1, \quad C_1 = \frac{\sqrt{2}}{\pi R_s} C_1, \quad B_2 = -\frac{1}{\pi R} B_2, \quad C_2 = -\frac{1}{\pi R_s} C_2 , \tag{3.9}$$

after calculating, we find:

$$\frac{\partial^2 A_1}{\partial t'^2} = -2\frac{V_a}{k^2}\frac{\partial A_1}{\partial t'} - \left(\frac{V_a^2}{k^4} + \mathrm{Pr}^2 T - R\,\mathrm{Pr}\,\Phi + Rs\,\mathrm{Pr}\,\Phi\right) A_1 + \mathrm{Pr}\,\Phi A_1 B_2 +$$
$$-\mathrm{Pr}\,\Phi \frac{1}{\pi R_S^*} A_1 C_2 + \mathrm{Pr}\,\Phi\left(\frac{V_a}{k^2} - 1\right)\tilde{B}_1 - \mathrm{Pr}\,\Phi\left(\frac{V_a}{k^2} - \frac{1}{Le}\right)\tilde{C}_1, \tag{3.10}$$

$$\frac{\partial \tilde{B}_1}{\partial t'} = -\tilde{B}_1 + R\tilde{A}_1 + A_1 B_2, \tag{3.11}$$

$$\frac{\partial \tilde{B}_2}{\partial t'} = -b\tilde{B}_2 - A_1 B_1, \tag{3.12}$$

$$\frac{\partial \tilde{C}_1}{\partial t'} = -\frac{1}{Le}\tilde{C}_1 + Rs\tilde{A}_1 + A_1 C_2, \tag{3.13}$$

$$\frac{\partial C_2}{\partial t'} = -\frac{b}{Le}\tilde{C}_2 - A_1 C_1. \tag{3.14}$$

Let's make the following variable changes:

$$A_1 = X\sqrt{b(R-1)}, \quad \tilde{B}_1 = Y\sqrt{b(R-1)}, \quad C_1 = U\sqrt{b(R-1)},$$
$$B_2 = Z(R-1), \quad C_2 = V(R-1) . \tag{3.15}$$

This gives us the following system of nonlinear equation:

$$\begin{cases} \frac{dX}{dt} = W, \\ \frac{dY}{dt} = RX - (R-1)XZ - Y, \\ \frac{dZ}{dt} = b(XY - Z), \\ \frac{dU}{dt} = RsX - (R-1)XV - \frac{1}{Le}U, \\ \frac{dV}{dt} = b\left(XU - \frac{1}{Le}V\right), \\ \frac{dW}{dt} = -2\frac{V_a}{k^2}W - \left(\frac{V_a^2}{k^4} + Pr^2T - RPr\Phi + RsPr\Phi\right)X - Pr\Phi(R-1)XZ + \\ +Pr\Phi(R-1)XV + Pr\Phi\left(\frac{V_a}{k^2} - 1\right)Y - Pr\Phi\left(\frac{V_a}{k^2} - \frac{1}{Le}\right)U. \end{cases} \tag{3.16}$$

When we are in the non-porous case ($\Phi = 1$) and without rotation ($Ta = 0$), the six-dimensional system obtained reduces to the five-dimensional system obtained by Idris *et al.* [13].

Dissipation is an evident property of the system (3.16). The flow divergence is:

$$\nabla V = \frac{dX'}{dX} + \frac{dY'}{dY} + \frac{dZ'}{dZ} + \frac{dU'}{dU} + \frac{dV'}{dV} + \frac{dW'}{dW} = -\left(1 + b + \frac{1}{Le} + \frac{b}{Le} + \frac{2Va}{k^2}\right). \tag{3.17}$$

We note that $\nabla V < 0$. This ensures, the present model is dissipative and possesses bounded solutions in phase plane. The detailed dynamic evolutions of the non-linear system (3.16) will be known from the analysis of the stability of the equilibrium points. They are determined by considering the amplitudes as independent ot time. This equivalent to writing:

$$\begin{cases} \frac{dX}{dt} = 0 \\ \frac{dY}{dt} = 0 \\ \frac{dZ}{dt} = 0 \\ \frac{dU}{dt} = 0 \\ \frac{dV}{dt} = 0 \\ \frac{dW}{dt} = 0 \end{cases} \Leftrightarrow \begin{cases} W_* = 0 \\ RX_* - (R-1)X_*Z_* - Y_* = 0 \\ b(X_*Y_* - Z_*) = 0 \\ RsX_* - (R-1)X_*V_* - \frac{1}{Le}U_* = 0 \\ b\left(X_*U_* - \frac{1}{Le}V_*\right) = 0 \\ -2\frac{Va}{k^2}W_* - \alpha_1 X_* - \alpha_2 X_*Z_* + \alpha_2 X_*V_* + \alpha_3 Y_* - \alpha_4 U_* = 0 \end{cases} \Leftrightarrow \begin{cases} X_* = X_* \\ Y_* = \frac{RX_*}{1+(R-1)X_*^2} \\ Z_* = \frac{RX_*^2}{1+(R-1)X_*^2} \\ U_* = \frac{R_S X_* Le}{1+(R-1)Le^2X_*^2} \\ V_* = \frac{R_S Le^2 X_*^2}{1+(R-1)Le^2X_*^2} \\ W_* = 0 \end{cases}, \tag{3.18}$$

where: $\alpha_1 = \frac{V_a^2}{k^4} + \Pr^2 T - R\Pr\Phi + Rs\Pr\Phi$, $\alpha_2 = \Pr\Phi(R-1)$,

$\alpha_3 = \Pr\Phi\left(\frac{V_a}{k^2} - 1\right)$ and $\alpha_4 = \Pr\Phi\left(\frac{V_a}{k^2} - \frac{1}{Le}\right)$.

We can see that the system has a trivial point fixe:

$$(X_0, Y_0, Z_0, U_0, V_0, W_0) = (0, 0, 0, 0, 0, 0), \tag{3.19}$$

and as for non-trivial solutions, we opted for the special case where the amplitudes X and Y are equal and found two other fixed points:

$$(X_1, Y_1, Z_1, U_1, V_1, W_1) = \left(1, 1, 1, \frac{Rs}{(R-1)Le + \frac{1}{Le}}, \frac{LeRs}{(R-1)Le + \frac{1}{Le}}, 0\right), \tag{3.20}$$

$$(X_2, Y_2, Z_2, U_2, V_2, W_2) = \left(-1, -1, 1, -\frac{Rs}{(R-1)Le + \frac{1}{Le}}, \frac{LeRs}{(R-1)Le + \frac{1}{Le}}, 0\right). \tag{3.21}$$

These fixed points satisfy the following condition:

$$\frac{Rs}{(R-1)Le + \frac{1}{Le}} = \frac{(\alpha_1 - \alpha_4) + \alpha_2}{\alpha_2 Le - \alpha_4}, \tag{3.22}$$

$$J = \begin{pmatrix} 0 & 0 & 0 & 0 & 0 & 1 \\ R-(R-1)Z & -1 & -(R-1)X & 0 & 0 & 0 \\ bY & bX & -b & 0 & 0 & 0 \\ R_s - (R-1)V & 0 & 0 & -\frac{1}{Le} & -(R-1)X & 0 \\ \lambda U & 0 & 0 & bX & -\frac{b}{Le} & 0 \\ -\alpha - \beta Z - \beta V & \gamma & -\beta X & -\delta & \beta X & -\frac{2Va}{k^2} \end{pmatrix}. \tag{3.24}$$

Using the Jacobian matrix around the particular equilibrium, the characteristic equation around the conducting phase solution is give by:

$$\sigma^6 + c_5\sigma^5 + c_4\sigma^4 + c_3\sigma^3 + c_2\sigma^2 + c_1\sigma + c_0 = 0, \tag{3.25}$$

where:

$$C_0 = \beta L_e^{*2} b^2 R V_1 X_1^2 + L_e^{*2} R\alpha b^2 X_1^2 + L_e^{*2} R b^2 \beta X_1^2 + L_e^{*2} R b^2 \gamma X_1 Y_1 + \gamma L_e^{*2} R b^2 Z_1 - L_e^{*2} R b^2 Y_1 +$$
$$-L_e^{*2} b^2 \beta V_1 X_1^2 + L_e^{*2} b^2 \beta V_1 - L_e^{*2} \alpha b^2 \beta X_1^2 + L_e^{*2} b^2 \beta X_1 Y_1 - L_e^{*2} b^2 \gamma X_1 Y_1 + L_e^{*2} b^2 \beta Z_1 - L_e^{*} b^2 \gamma Z_1 +$$
$$+L_e^{*2} b^2 \alpha - L_e^{*} R^2 b^2 \delta V_1 X_1^2 + L_e^{*} R R_S b^2 \delta X_1^2 - L_e^{*} R b^2 \beta U_1 X_1^3 + 2L_e^{*} R b^2 \delta V_1 X_1^2 - L_e^{*} R b^2 \delta V_1 +$$
$$-L_e^{*} R_S b^2 \delta X_1^2 + L_e^{*} R_S b^2 \delta + L_e^{*} b^2 \beta U_1 X_1^3 - L_e^{*} b^2 \beta U_1 X_1 - L_e^{*} b^2 \delta V_1 X_1^2 + L_e^{*} b^2 \delta V_1 - R^2 b^2 \delta U_1 X_1^3 +$$
$$+2R^2 b^2 \beta V_1 X_1^4 + R^2 b^2 \alpha X_1^4 + R^2 b^2 \beta X_1^4 + R^2 b^2 \gamma X_1^3 Y_1 + R^2 b^2 \gamma X_1^2 Z_1 - R^2 b^2 \gamma X_1^2 - R R_S b^2 \beta X_1^4 +$$
$$+2R b^2 \delta U_1 X_1^3 - R b^2 \delta U_1 X_1 - 4R b^2 \beta V_1 X_1^4 + 2R b^2 \beta V_1 X_1^2 + 2R b^2 \alpha X_1^4 - R b^2 \beta X_1^4 + R^2 b^2 \beta X_1^3 Y_1 +$$
$$-2R b^2 \gamma Y_1 X_1^3 + R b^2 \beta Z_1 X_1^2 - 2R b^2 \gamma Z_1 X_1^2 + R b^2 \alpha X_1^2 + R_S b^2 \beta X_1^4 - R_S b^2 \beta X_1^2 - b^2 \delta U_1 X_1^3 +$$
$$+b^2 \delta U_1 X_1 + 2b^2 \beta V_1 X_1^4 - 2b^2 \beta V_1 X_1^2 + \alpha b^2 X_1^4 + b^2 \gamma Y_1 X_1^3 - b^2 \beta Z_1 X_1^2 + b^2 Z_1 V_1 X_1^2 - b^2 \alpha X_1^2,$$

$$C_2 = 2L_e^{*2} V_a b^2 + 2L_e^{*2} V_a^* b + L_e^{*2} R V_{a\,a}^* b^2 X_1^2 + L_e^{*2} b \beta V_1 - L_e^{*2} b^2 X_1^2 + L_e^{*2} b \beta Z_1 + L_e^{*2} \alpha b + L_e^{*2} b^2 +$$
$$+2L_e^{*} R V_a^* b^2 X_1^2 + 2L_e^{*} R V_a^* b X_1^2 - 2L_e^{*} V_a^* b^2 X_1^2 - 2L_e^{*} V_{a\,a}^* b X_1^2 + 2L_e^{*} V_a^* b^2 + 2L_e^{*} V_a^* b - L_e^{*} R b \delta V_1 +$$
$$+L_e^{*} R b \gamma Z_1 + L_e^{*} R \gamma Z_1 + L_e^{*} R \gamma Z_1 - L_e^{*} R b \gamma - L_e^{*} R \gamma + L_e^{*} R_S b \delta - L_e^{*} b \beta U_1 X_1 + L_e^{*} V_1 b^2 \beta + 2L_e^{*} b \beta V_1 +$$
$$+L_e^{*} \beta \delta V_1 + L_e^{*} \beta V_1 + L_e^{*} b^2 \beta X_1 Y_1 + L_e^{*} b \beta X_1 Y_1 + L_e^{*} b^2 \beta Z_1 + 2L_e^{*} b \beta Z_1 - L_e^{*} b \gamma Z_1 + L_e^{*} \gamma Z_1 - L_e^{*} \gamma Z_1 +$$
$$+L_e^{*} \alpha b^2 + 2L_e^{*} \alpha b + L_e^{*} \alpha + 2R V_a^* b^2 X_1^2 + 2R V_a^* b X_1^2 - 2V_a^* b^2 X_1^2 - 2R V_a^* b X_1^2 + R^2 b^2 X_1^4 +$$
$$-R b \delta U_1 X_1 + 3R b \beta V_1 X_1^2 - R b \beta V_1 - R \delta V_1 - 2R b^2 X_1^2 + R b \beta Z_1 X_1^2 + 2R \alpha b X_1^2 + R b^2 X_1^2 +$$
$$+R b \beta X_1^2 + R b \gamma X_1 Y_1 + R b \gamma Z_1 - R b \gamma - R_S b \beta X_1^2 + R_S b \delta + R_S \delta - b^2 \beta U_1 X_1 - b \beta U_1 X_1 +$$
$$+b \delta X_1 U_1 - 3b \beta V_1 X_1^2 + b \beta V_1 + b \delta V_1 + \delta V_1 + b^2 X_1^4 - b \beta Z_1 X_1^2 - \alpha b X_1^2 - b^2 X_1^2 + b \beta X_1 Y_1 +$$
$$-b \gamma X_1 Y_1 + b \beta Z_1 - b \gamma Z_1 + \alpha b,$$

$$C_3 = 2L_e^{*2} V_a^* b + L_e^{*2} b^2 + L_e^{*2} b + 2L_e^{*} V_a^* b^2 + 4L_e^{*} V_a^* b + 2L_e^{*} V_a^* + L_e^{*} R b^2 X_1^2 + L_e^{*} R b X_1^2 + L_e^{*} V_1 b \beta +$$
$$+L_e^{*} V_1 \beta - L_e^{*} b^2 X_1^2 - L_e^{*} b X_1^2 + L_e^{*} b \beta Z_1 + L_e^{*} \beta Z_1 + L_e^{*} \alpha \beta + L_e^{*} \alpha + L_e^{*} b^2 + L_e^{*} b + 4R V_a^* b X^2 +$$
$$-4V_a^* b X_1^2 + 2V_a^* b - R \delta V_1 + R b^2 X_1^2 + R b X_1^2 + R \gamma Z_1 - R \gamma + R \delta - b \beta X_1 U_1 + b \beta V_1 + \beta V_1 + \delta V_1 +$$
$$-b^2 X_1^2 - b X_1^2 + b \beta X_1 Y_1 + b \beta Z_1 + \beta Z_1 - \gamma Z_1 + \alpha V_1 + \alpha,$$

$$C_4 = L_e^{*2} b + 2L_e^{*} V_a^* b + 2L_e^{*} V_a^* + L_e^{*} b^2 + 2L_e^{*} b + 2R b X_1^2 +$$
$$+L_e^{*} + 2V_a^* b + 2V_a^* + \beta V_1 - 2b X_1 + \alpha + b,$$

$$C_5 = L_e^{*} b + L_e^{*} + 2V_a^* + b + 1,$$

and

$$C_6 = 1 \quad \text{with:} \quad L_e^{*} = \frac{1}{L_e}, \quad V_a^* = \frac{V_a}{k^2}.$$

Substituting $\sigma = i\omega$ in Eq.(3.25), separating real and imaginary parts and equating the imaginary part to zero, we obtain the expression for ω^2 given by:

$$\omega^2 = \frac{c_4 \pm \sqrt{c_4^2 - 4c_2c_6}}{2c_2}. \tag{3.26}$$

Substituting Eq.(3.26) in the real part of the Eq.(3.25) we get,

$$c_6\left(\omega^2\right)^3 + c_4\left(\omega^2\right)^2 + c_5\omega^2 + c_0 = 0. \tag{3.27}$$

Solving the Eq.(3.27) with respect to R numerically, we obtain the value of the Hopf-Rayleigh number. Having completed the analytical framework of the problem, we now proceed to present and interpret the results obtained in the following section.

The Runge-Kutta method is one of the most effective methods for solving initial value problems of differential equations [17]. This method is used to construct an accurate numerical method for system (3.16). The first amplitude of the initial value of the system is of the first order. Referring to the most commonly used Runge-Kutta formula, we obtain the following formula for the amplitude :

$$\begin{cases} X_{\tau_{n+1}} = X_{\tau_n} + \frac{1}{6}\left(K_1 + 2K_2 + 2K_3 + K_4\right), \\ K_{1,X} = h.f_X\left(\tau_n, X_n, Y_n, Z_n, U_n, V_n, W_n\right), \\ K_{2,X} = h.f_X\left(\tau_n + \frac{1}{2}h,\ X_n + \frac{1}{2}K_1, Y_n + \frac{1}{2}K_1,\ Z_n + \frac{1}{2}K_1,\ U_n + \frac{1}{2}K_1,\ V_n + \frac{1}{2}K_1,\ W_n + \frac{1}{2}K_1\right), \\ K_{3,X} = h.f_X\left(\tau_n + \frac{1}{2}h,\ X_n + \frac{1}{2}K_2, Y_n + \frac{1}{2}K_2, Z_n + \frac{1}{2}K_2, U_n + \frac{1}{2}K_2, V_n + \frac{1}{2}K_2, W_n + \frac{1}{2}K_2\right), \\ K_{4,X} = h.f_X\left(\tau_n + \frac{1}{2}h,\ X_n + K_3, Y_n + +K_3, Z_n + K_3, U_n + K_3, V_n + K_3, W_n + K_3\right). \end{cases}$$

(3.28)

The same technique is applied to other amplitudes, and a Fortran code is written for the numerical calculations. The transition to chaos of the system is determined by the Lyapunov exponent defined by:

$$Lya = \lim_{\tau\to\infty} \frac{\ln\sqrt{(dX)^2 + (dY)^2 + (dZ)^2 + (dU)^2 + (dV)^2 + (dW)^2}}{\tau}, \tag{3.29}$$

with dX, dY, dW, dU, dV and dW the variation of C, Y, Z, U, V and W respectively. The system is chaotic when the largest Lyapunov exponent is positive, periodic when it is negative and quasi-periodic when it is zero.

4. Results and discussion

In order to examine and study the various transitions in the thermosolutal convection of a Newtonian fluid rotating in an isotropic porous medium, numerical simulations were performed. The fourth-order Runge-Kutta method is used to numerically solve the nonlinear system (3.16), and the companion polynomial matrix of the Lapack method is used to solve the eigenvalue equations using the Fortran language. In order to better understand the dynamic behavior of Rayleigh-Bénard convection with double diffusion in a porous medium, we will analyze a generalized sixth-order modified Lorenz model, represented by system (3.16). Unlike the classical Lorenz model with two nonlinear terms, this model incorporates four nonlinearities. The Lorenz model is scaled so that when porosity is considered equal to 1 and the rotation and solute concentration parameters are considered zero, the classical Lorenz model is recovered. The model presented also satisfies the properties of the classical Lorenz model proposed by Lorenz [18]. The dynamic system has two fixed points, the first related to the trivial solution representing the conduction state and the other points related to the non-trivial solutions corresponding to the convection state. To find the polynomial equations with eigenvalues, we use the 6×6 Jacobian matrix given in Eq.(3.16). The trivial equilibrium point is substituted into the time-dependent amplitudes and simplified by considering the characteristic equation to study the loss of conduction in the system. Due to the complexity of the problem, it is not possible to derive an explicit analytical expression for which the Hopf-Rayleigh bifurcation would be obtained, so it is calculated numerically. We will now examine the effects of the different regimes in more detail. Figures 2 to 11 show the bifurcation diagrams and the largest Lyapunov exponents for $Va = 100$, $\phi = 0.96$ and $0 < R < 150$.

Taking the Lewis number $Le = 0.1$, the rescaled Rayleigh number $Rs = 15$, and the reduced Taylor number $T = 0.1$, we see in Fig.2 that the system exhibits regular attractors (at one point), but that the value of the amplitude Z increases as the rescaled Rayleigh number increases, up to approximately $R \simeq 50$. This is when the bifurcation occurs, followed by a doubling of the periods until just after $R = 85$, where the system is chaotic. With the increase in R, we observe a domain of intermittency $(112 < R < 120)$. All these predictions are in perfect agreement with the corresponding Lyapunov exponent constructed in Fig.3. It should be noted that the system is not completely chaotic for all values of the rescaled thermal Rayleigh number greater than 85, and we will discuss this using a phase portrait diagram.

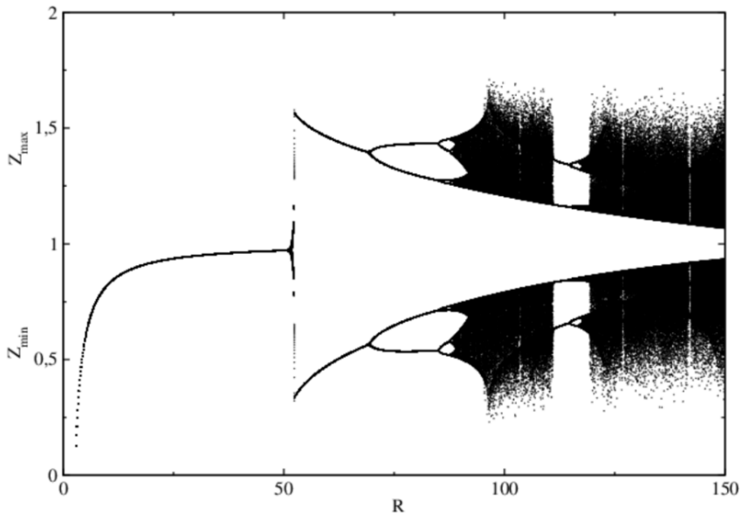

Fig.2. Bifurcation diagram of C as function of R for $V_a = 100$, $Le = 0.1$, $Rs = 15$, $\phi = 0.96$ and $T = 0.1$.

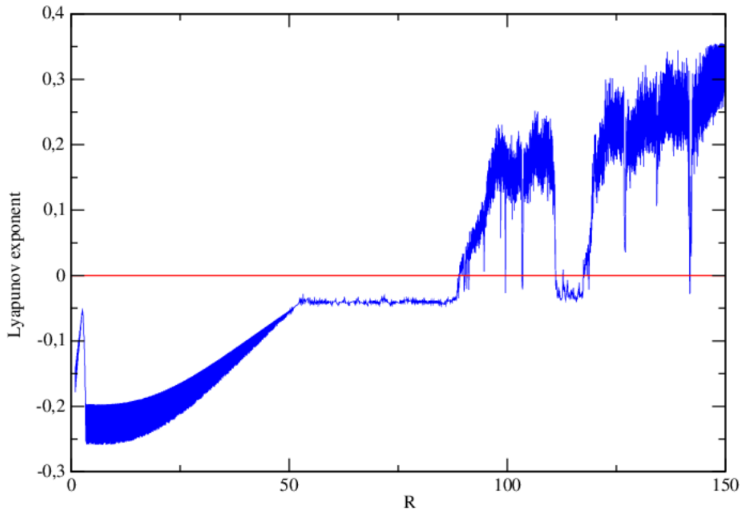

Fig.3. Lyapunov exponent for $V_a = 100$, $Le = 0.1$, $Rs = 15$, $\phi = 0.96$ and $T = 0.1$.

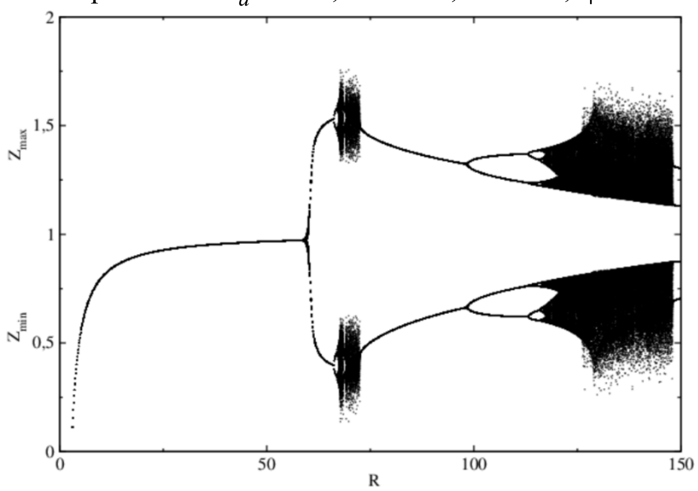

Fig.4. Bifurcation diagram of C as function of R for $V_a = 100$, $Le = 0.1$, $Rs = 15$, $\phi = 0.96$ and $T = 0.3$.

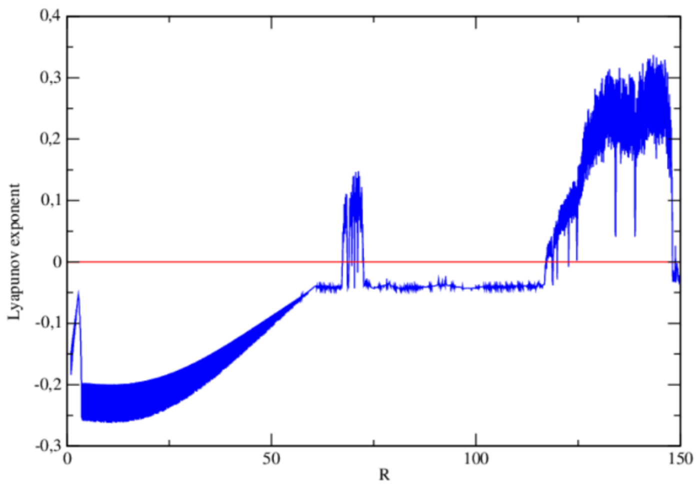

Fig.5. Lyapunov exponent for $V_a = 100$, $Le = 0.3$, $Rs = 15$, $\phi = 0.96$ and $T = 0.1$.

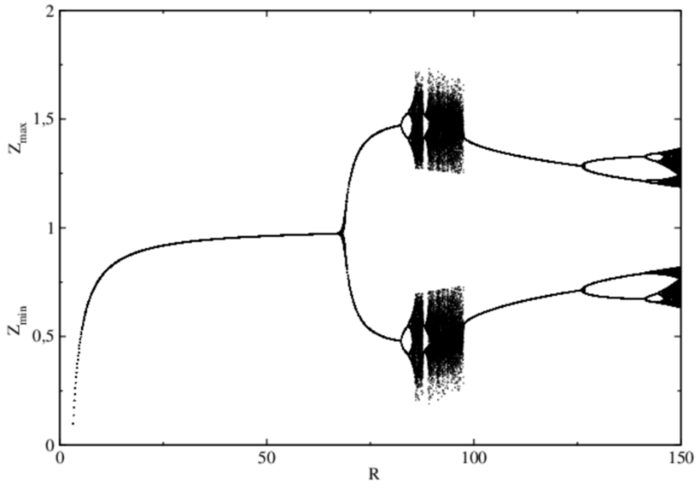

Fig.6. Bifurcation diagram of C as function of R for $V_a = 100$, $Le = 0.1$, $Rs = 15$, $\phi = 0.96$ and $T = 0.5$.

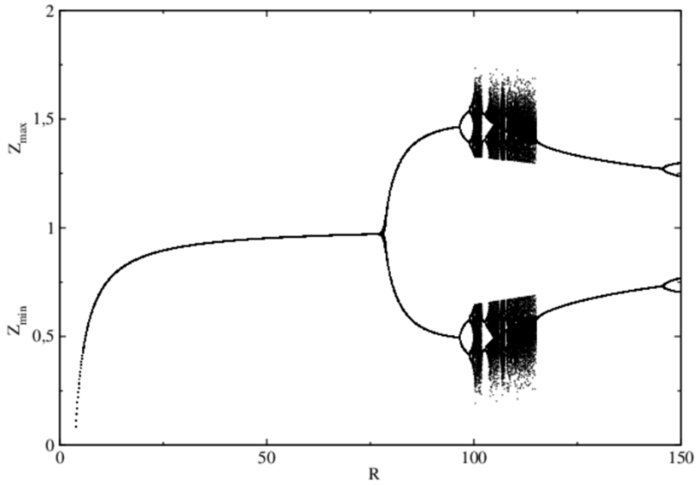

Fig.7. Bifurcation diagram of C as function of R for $V_a = 100$, $Le = 0.1$, $Rs = 25$, $\phi = 0.96$ and $T = 0.1$.

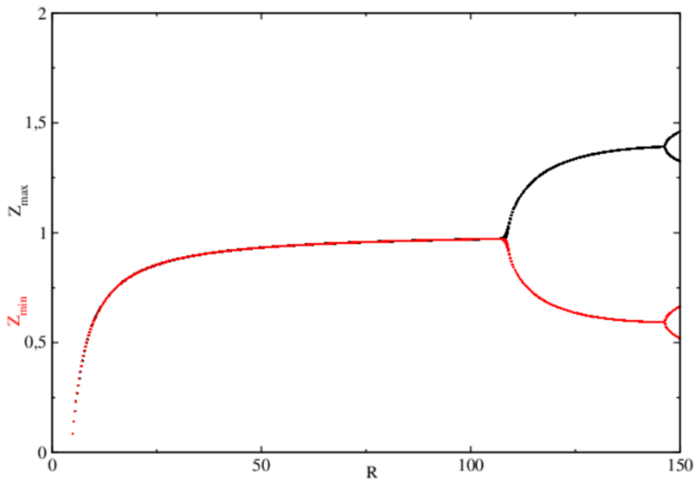

Fig.8. Bifurcation diagram of C as function of R for $V_a = 100$, $Le = 0.1$, $Rs = 35$, $\phi = 0.96$ and $T = 0.1$.

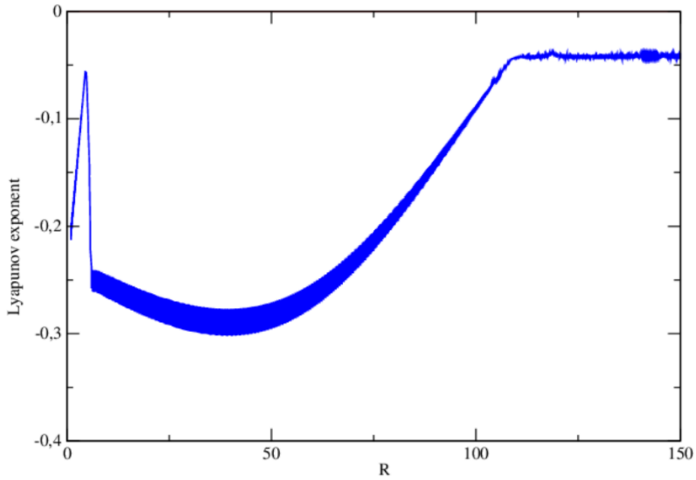

Fig.9. Lyapunov exponent for $V_a = 100$, $Le = 0.1$, $Rs = 35$, $\phi = 0.96$ and $T = 0.1$.

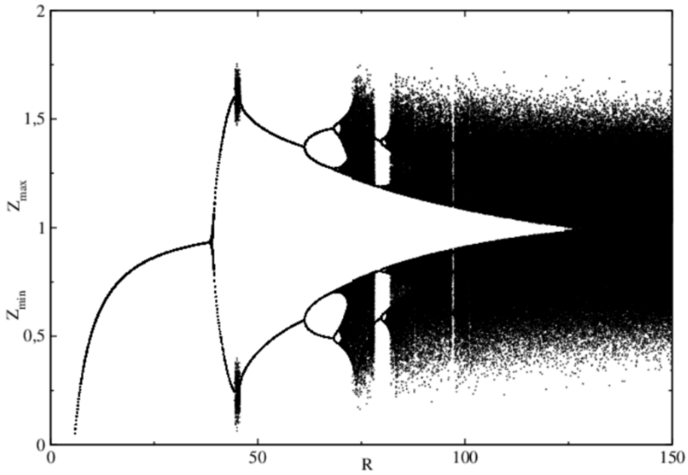

Fig.10. Bifurcation diagram of C as function of R for $V_a = 100$, $Le = 0.3$, $Rs = 15$, $\phi = 0.96$ and $T = 0.1$.

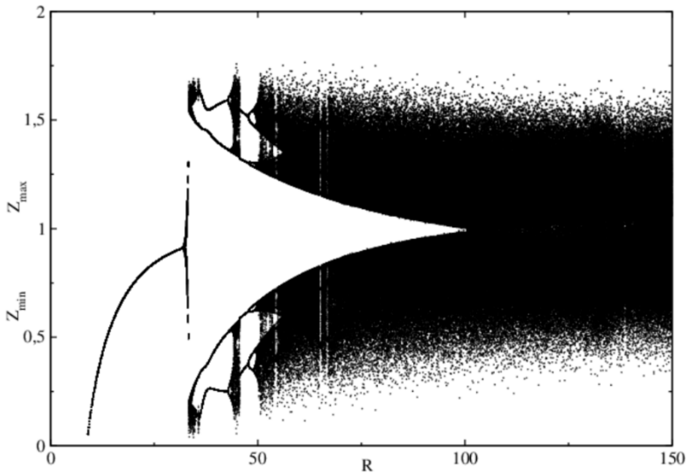

Fig.11. Bifurcation diagram of C as function of R for $V_a = 100$, $Le = 0.5$, $Rs = 15$, $\phi = 0.96$ and $T = 0.1$.

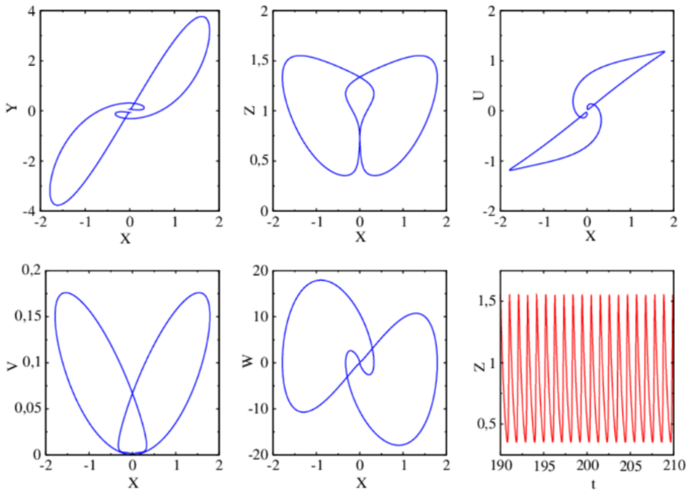

Fig.12. Phase space and times history for $V_a = 100$, $Le = 0.1$, $Rs = 15$, $\phi = 0.96$, $T = 0.1$ and $R = 53$.

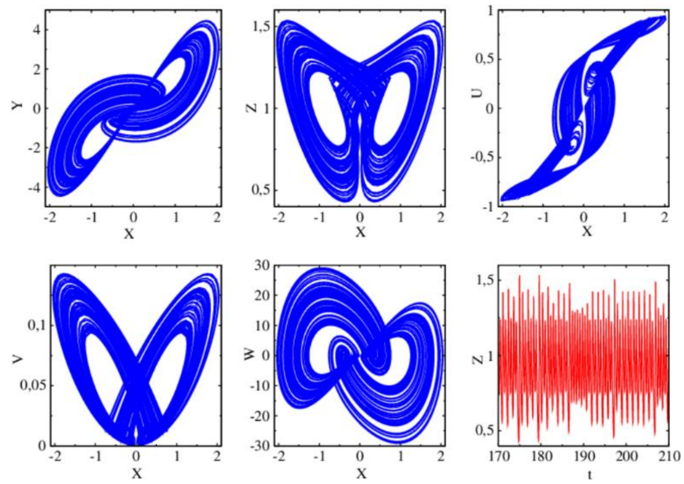

Fig.13. Phase space and times history for $V_a = 100$, $Le = 0.1$, $Rs = 15$, $\phi = 0.96$, $T = 0.1$ and $R = 95$.

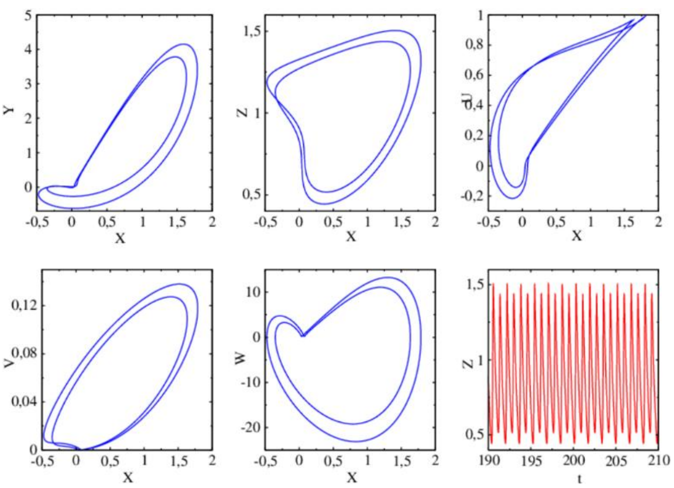

Fig.14. Phase space and times history $V_a = 100$, $Le = 0.1$, $Rs = 15$, $\phi = 0.96$, $T = 0.5$ and $R = 83$.

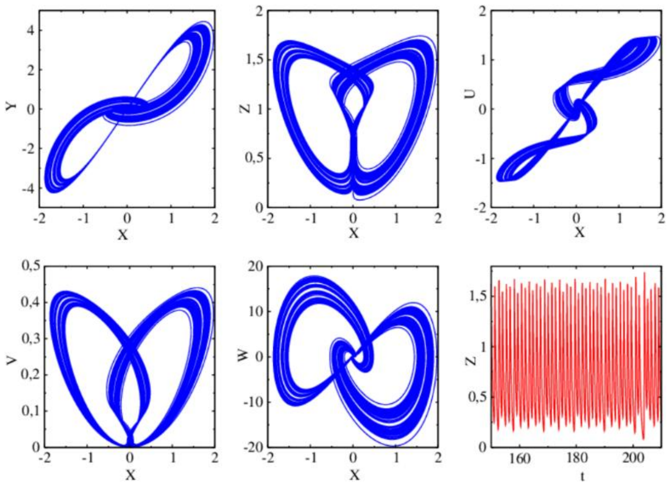

Fig.15. Phase space and times history for $V_a = 100$, $Le = 0.3$, $Rs = 15$, $\phi = 0.96$, $T = 0.1$ and $R = 45$.

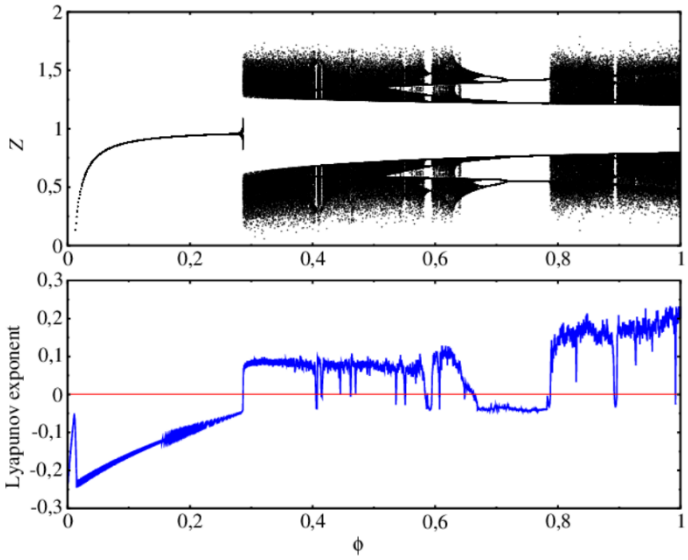

Fig.16. Bifurcation diagram of Z as function of ϕ and it corresponding Lyapunov exponent for $V_a = 100$, $Le = 0.1$, $Rs = 15$, $R = 100$ and $T = 0.1$.

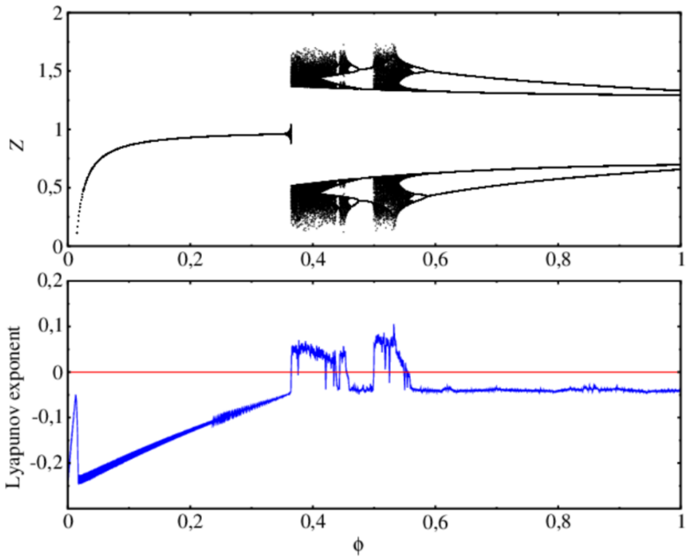

Fig.17. Bifurcation diagram of Z as function of ϕ corresponding Lyapunov exponent for $V_a = 100$, $Le = 0.1$, $Rs = 15$, $R = 100$ and $T = 0.3$.

When we fix the Lewis number $(Le = 0.1)$ and the solute Rayleigh number $(Rs = 15)$ while increasing the rescaled Taylor number Ta from 0.1 to 0.3, chaotic behavior appears in the range $66 < R < 73$. After $R = 73$, as shown in Fig.4 and confirmed by Fig.5, the regular attractors expand to approximately $R = 115$ and then chaotic behavior takes over. We can therefore deduce that increasing the value of the rotational force intensity precipitated the onset of chaos in the system while reducing its persistence. The same scenario occurs when the Taylor number is increased to 0.5, as shown in the bifurcation diagram constructed in Fig.5 and confirmed by the Lyapunov function in Fig.6. We now seek to verify the effect of particle concentration on fluid flow. To this end, we varied the Rayleigh number of the solute, with all other parameters fixed, taking $Rs = 25$ and $Rs = 35$ in Figs 7-8, respectively. We observe that chaos is delayed. We can therefore conclude that increasing the Rayleigh number of the solute delays the onset of chaos in the system. Fig.9 confirms the dynamics observed in Fig.8. To study the effect of the Lewis number on the dynamics of the system, we took $Le = 0.3$ (Fig.10) and $Le = 0.5$ (Fig.11).

Comparing the data in these figures with those in Fig.2, it appears that the Lewis number accelerates the onset of chaotic convection in the fluid. In order to highlight the different transitions that occur in the system, we constructed phase spaces and time evolutions. Indeed, for $Va = 100$, $Le = 0.1$, $Rs = 15$, $\phi = 0.96$, $T = 0.1$, $R = 53$ and $R = 95$, Fig.12 shows regular behavior with a period of 1, and Fig.13 shows chaotic behavior of the system, as indicated in Fig.2. Similarly, in line with the predictions in Fig.3, the regular behavior of period 2 and the chaotic behavior are shown in Figs 14-15 for $R = 83$ and $R = 45$, respectively.

Furthermore, following the same logic as before, we considered porosity as a bifurcation parameter, taken between 0 and 1, choosing $T = 0.1$ and $T = 0.3$ to construct the bifurcation diagrams shown in Figs 16-17, respectively. The different transitions observed show that porosity has a considerable effect on thermosolutal flow. Its choice is therefore crucial in the thermoconvection process, as we can obtain regular, periodic, or chaotic behavior depending on how the other parameters are defined.

5. Conclusions

This article explores the instability of double diffusion convection in a porous cavity where the solute is added from the bottom plate. Nonlinear stability analysis is performed to study the chaotic and periodic behaviors of double diffusion in Rayleigh-Bénard convection in a porous medium, using a robust six-dimensional system. Based on this research, we conclude that the presence of a solute concentration in a Newtonian fluid subjected to a rotational force delays the onset of chaos and periodic convection compared to the case of a Newtonian fluid. On the other hand, the Lewis number accelerates the onset of chaotic convection, thereby destabilizing the system. Porosity is a key parameter whose choice has a considerable effect on the dynamics of thermosolutal flow. To further the research, it would be interesting to use a simple neural network approach to estimate the largest Lyapunov exponent (LLE) directly from a single scalar time series. Studying the coexistence of attractors and fractional order on the resulting 6D system would add a significant contribution to this work.

Data availability

No data were used to support this study.

Conflicts of interest

The authors declare that they have no conflict of interest.

Acknowledgments

The authors gratefully acknowledge the anonymous referees whose helpful criticisms, comments, and suggestions enhance the content and quality of the article. They thank also Doctor Sèmako Justin Dèdèwanou for his frank collaboration.

Nomenclature

c – critical
Da – Darcy number
$\vec{e}_n$ – unit vector normal to the boundary
$\vec{g}$ – acceleration vector of gravity, gravity intensity $\left[m\,s^{-2}\right]$
k – permeability $\left[m^2\right]$
Le – Lewis number
P – pressure $[Pa]$
Pr – Prandtl number
Ra – thermal Rayleigh number
Rs – solute Rayleigh number
Ta – Taylor number
T – reduced Taylor number
t – time $[s]$
Tc – hot temperature $[°C]$
To – cold temperature $[°C]$
T – temperature $[°C]$
(u,v,w) – components of the velocity vector
Va – Vadasz number
$\vec{v}$ – velocity vector
(x,y,z) – cartesian coordinates
(X,Y,Z) – coordinates of the fixed point
α_T – thermal diffusivity of the fluid in $\left[m^2 s^{-1}\right]$

μ – dynamic viscosity in $\left[Kg\, m^{-1} s^{-1}\right]$

ρ – density in $\left[Kg\, m^{-3}\right]$

∇ – gradient

Φ – porosity of the medium

* – dimensionless

References

[1] Nield D.A. and Bejan A. (2006): *Convection in Porous Media*.– 3rd Edn, Springer, New York.

[2] De Paoli M. (2023): *Convective mixing in porous media: a review of Darcy, pore-scale and Hele-Shaw studies*.– Eur. Phys. J. E, vol.46, no.129, pp.2-26, DOI:10.1140/epje/s10189-023-00390-8.

[3] Virupaksha A.G., Nagel T., Lehmann F., Rajabi M.M., Hoteit H., Fahs M. and Le Ber F. (2024): *Modeling transient natural convection in heterogeneous porous media with Convolutional Neural Networks*.– International Journal of Heat and Mass Transfer, vol.222, pp.125149, DOI:10.1016/j.ijheatmasstransfer.2023.125149.

[4] Nield D.A. (1968): *Onset of thermohaline convection in a porous medium*.– Water Resour. Res., vol.4, pp.553-560.

[5] Umavathi J.C. and Bég O.A. (2020): *Modeling the onset of thermosolutal convective instability in a non-Newtonian nanofluid-saturated porous medium layer*.– Chinese Journal of Physics, vol.68, pp.147-167, DOI:10.1016/j.cjph.2020.09.014.

[6] Taunton J.W., Lightfoot E.N. and Green T. (1972): *Thermohaline instability and salt fingers in a porous medium*.– Phys. Fluids, vol.15, pp.748–753.

[7] Mojtabi A. and Charrier-Mojtabi M.C. (2000): *Double-diffusive convection in porous media*.– In: K Vafai (Ed.), Handbook of Porous Media, Dekker, New York, pp.559-603.

[8] Mamou M. (2002): *Stability analysis of double-diffusive convection in porous enclosures*.– In: D B Ingham, I Pop (Eds.), Transport Phenomena in Porous Media II, Elsevier, Oxford, pp.113-154.

[9] Huppert H.E. (1976): *Transitions in double-diffusive convection*.– Nature, vol.263, pp.20-22.

[10] Huppert H.E. (1977): *Thermosolutal Convection*.– In Problems of Stellar Convection (ed. E. A. Spiegel & J.-P. Zahn), Lecture Notes in Physics, Springer, vol.71, pp.239-254.

[11] Knobloch E., Moore D.R., Toomre J. and Weiss N.O. (1986): *Transitions to chaos in two dimensional double-diffusive convection*.– Journal of Fluid Mechanics, vol.166, pp.409-448.

[12] Sibgatullin I.N., Gertsenstein S.Ja. and Sibgatullin N.R. (2003): *Some properties of two-dimensional stochastic regimes of double-diffusive convection in plane layer*.– Chaos, vol.13, no.4, pp.1231-1241, DOI:10.1063/1.1615911.

[13] Idris R., Siri Z. and Hashim I. (2013): *On a five-dimensional chaotic system arising from double-diffusive convection in a fluid layer*.– vol.2013, No.1, pp.428327, DOI:10.1155/2013/428327.

[14] Sharma R.P., Shaw S., Mishra S.R. and Tinker S. (2021): *Exploration of radiative heat on magnetohydrodynamic rotating fluid flow through a vertical sheet*.– Heat Transfer, vol.50, No.8, pp.8506-8524, DOI:10.1002/htj.22287.

[15] Mohanty D., Mahanta G., Shaw S. and Katta R. (2024): *Entropy and thermal performance on shape-based 3D tri-hybrid nanofluid flow due to a rotating disk with statistical analysis*.– J. Therm. Anal. Calorim., vol.149, pp.12285-12306, DOI:10.1007/s10973-024-13592-9.

[16] Siddheshwar P.G., Kanchana C. and Laroze D. (2021): *A study of Darcy-Bénard regular and chaotic convection using a new local thermal non-equilibrium formulation*.– Physics of Fluids, vol.33, Article 044107, DOI:10.1063/5.0046358.

[17] Zheng L. and Zhang X. (2017): *Numerical Methods*.– In: Zheng, L. and Zhang, X., Eds., Modeling and Analysis of Modern Fluid Problems, Elsevier, pp.361-455, DOI:10.1016/b978-0-12-811753-8.00008-6

[18] Lorenz E.N. (1963): *Deterministic nonperiodic flow*.– Journal of Atmospheric Sciences, vol.20, no.2, pp.130-141.

Received: September 3, 2025
Revised: June 2, 2026